LA-UR-97- 1666

*Title:* IMPRESSION CREEP BEHAVIOR OF ATMOSPHERIC PLASMA SPRAYED AND HOT PRESSED $MOSI_2/SI_3N_4$

CONF-970929--

*Author(s):* KENDALL J. HOLLIS, MST-6
DARRYL P. BUTT, MST-6
RICHARD G. CASTRO, MST-6



*Submitted to:* PROCEEDINGS OF THE UNITED THERMAL SPRAY CONFERENCE HELD ON SEPTEMBER 15-18, 1997 IN INDIANAPOLIS



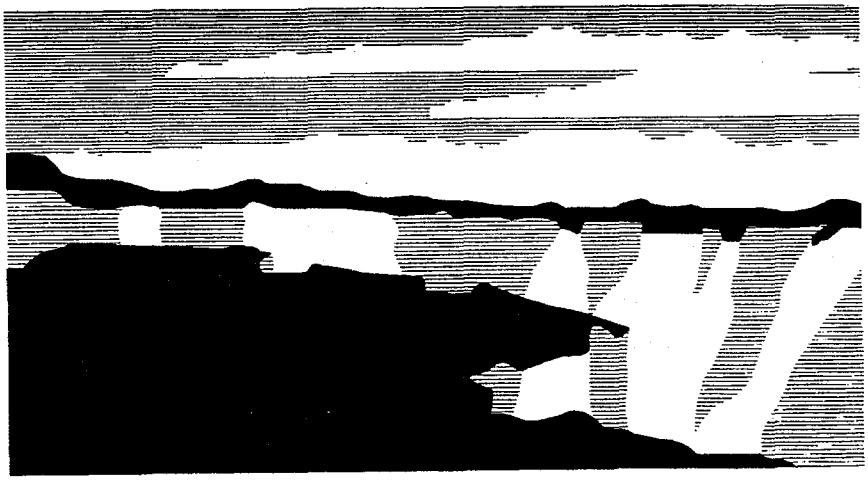

# DISCLAIMER

# Impression Creep Behavior of Atmospheric Plasma Sprayed and Hot Pressed $MoSi_2/Si_3N_4$

Kendall J. Hollis, Darryl P. Butt, Richard G. Castro

## Abstract

The use of $MoSi_2$ as a high temperature oxidation resistant structural material is hindered by its poor elevated temperature creep resistance. The addition of second phase $Si_3N_4$ holds promise for improving the creep properties of $MoSi_2$ without decreasing oxidation resistance. The high temperature impression creep behavior of atmospheric plasma sprayed (APS) and hot pressed (HP) $MoSi_2/Si_3N_4$ composites was investigated. Values for steady state creep rates, creep activation energies, and creep stress exponents were measured. Grain boundary sliding and splat sliding were found to be the dominant creep mechanisms for the APS samples while grain boundary sliding and plastic deformation were found to be the dominant creep mechanisms for the HP samples.

## Introduction

$MoSi_2$ HAS RECEIVED CONSIDERABLE attention as a structural material for elevated temperature oxidizing environments as a result of its unique combination of its high melting point (2030°C) and good oxidation resistance at elevated temperatures[1]. In an oxidizing environment, $MoSi_2$ oxidizes to $SiO_2$ and molybdenum oxide. The molybdenum oxide formed is volatilized leaving a pure, adherent $SiO_2$ protective layer on the $MoSi_2$ free surface which inhibits further oxidation [2,3,4]. However, for $MoSi_2$-based materials to be successfully employed in high temperature structural applications, the high temperature creep resistance must be improved. The composite approach with ceramic reinforcements such as SiC and $Si_3N_4$ has been shown to yield such improvements, with no significant reduction in the oxidation resistance of these materials [1].

The high temperature compressive creep behavior of low pressure plasma spray (LPPS) consolidated $MoSi_2$/SiC composite material has been characterized by *Jeng et al.*[5,6]. In these studies powders of $MoSi_2$ and SiC were blended followed by spray deposition. The SiC content of the samples was estimated to be 8.7 vol.%. The mechanisms for creep were observed to change as a function of increasing temperature from dislocation motion controlled by lattice diffusion to grain boundary sliding controlled by grain boundary diffusion. The transition temperature was found to be approximately 1300°C. Compression creep rates ranged from $7x10^{-7}$ to $6x10^{-4}$ $sec^{-1}$ for applied stress in the range of 20-100 MPa and test temperature range of 1100°C to 1500°C. Values for activation energy were found to be Q=300 kJ/mole for T<1300°C and Q=190 kJ/mole for T>1300°C. The change in creep mechanism was thought to be due to the softening of amorphous $SiO_2$ along grain boundaries at temperatures above 1300°C.

In the present study, a different approach has been taken to further improve the viability of $MoSi_2$ for use in high temperature structural components. The ceramic reinforcing phase chosen for the $MoSi_2$ is $Si_3N_4$. $MoSi_2$ and $Si_3N_4$ are thermodynamically stable compounds [7] and additions of $Si_3N_4$ to a $MoSi_2$ matrix significantly improve the intermediate temperature oxidation resistance of $MoSi_2$ and its elevated temperature mechanical properties [8]. Additionally, one study has found that hot pressed samples of $MoSi_2/Si_3N_4$ containing 10-20% $Si_3N_4$ exhibited superior high temperature strength compared to samples of $MoSi_2$/SiC containing 20-30% SiC [9]. In the present study, instead of mixing powders of $MoSi_2$ and $Si_3N_4$, a composite powder was used. The powder was produced by the self-propagating high-temperature synthesis (SHS) method. Details of the synthesis method and characterization of the powder are given elsewhere [10, 11]. The powder consists of small $Si_3N_4$ particles attached to the outer surface of larger $MoSi_2$ particles. Binding the $Si_3N_4$ to the $MoSi_2$ may give a more uniform distribution of the reinforcement in the $MoSi_2$ matrix and lessen the loss of $Si_3N_4$ by sublimation during deposition. Atmospheric plasma spraying (APS) was used instead of the more commonly used LPPS method for depositing $MoSi_2$. The cost savings of fabricating structural components by the APS method make their acceptance for industrial applications more attractive.

## Experimental Procedure

Samples for impression creep testing in this experiment were prepared from a $Si_3N_4$ reinforced $MoSi_2$ powder. The powder was manufactured by the high temperature reaction synthesis method by Exotherm, Inc., Camden, NJ. Each powder particle consisted of both $Si_3N_4$ and $MoSi_2$ with the $Si_3N_4$ distributed on the outer surface of the $MoSi_2$. The powder size distribution given by the manufacturer was -65μm +10μm. Samples were produced by atmospheric plasma spraying (APS). For comparison, hot pressed (HP) samples of the same powder were also tested. The APS parameters are shown in Table 1 and the HP parameters are shown in Table 2.

Impression creep testing as described in this study uses a cylindrical punch (SiC in this case) to indent the surface of the sample. This technique has been used by various investigators in the past [12,13]. The samples are tested in an air atmosphere furnace to provide the appropriate temperature. The general equation governing impression creep for a cylindrical punch is:

$$\dot{\varepsilon}_{ss}^{i} = \frac{v}{2a} = A(d)^{-m}\left(\frac{\sigma_{app}}{B}\right)^{n}\exp\left(\frac{-Q}{RT}\right) \qquad (1)$$

where $\dot{\varepsilon}_{ss}^{i}$ is the steady-state creep rate for impression creep, $v$ is the punch velocity, $2a$ is the punch diameter, $d$ is the grain size, $m$ is the grain size exponent, $\sigma_{app}$ is the applied stress, $B$ is a stress correction factor, $n$ is the stress exponent, $Q$ is the activation

energy, and $RT$ has the usual meaning. Finite element modeling [14] has determined the relation between $B$ and $n$ to be:

$$B = 2.5 \arctan [\, 1.86 ( n - 0.6 ) \,] - 0.47 \log n \qquad (2)$$

Test temperatures ranged from 1000°C to 1200°C and applied loads ranged from 260 MPa to 370 MPa. The sample loading direction was parallel to the spray direction or pressing direction for APS and HP samples respectively. Using Eq. 1 values for $n$ can be determined by applying an exponential curve fit to a plot of the creep rate versus the applied stress. Likewise, $Q$ is found by a linear curve fit of a plot of ln(creep rate) versus the reciprocal of absolute temperature.

## Results and Discussion

Image analysis of SEM and optical micrographs of the APS and HP samples were used to determine the porosity and composition of each material. The results of the image analysis are shown in Table 3. Fig. 1 shows the $MoSi_2$, $Si_3N_4$, and porosity in the APS sample. The APS sample lost silicon during the spraying process as is evidenced by its higher $Mo_5Si_3$ content compared to the HP sample. It has been shown that the $Mo_5Si_3$ can act as a reinforcing phase in the $MoSi_2$ matrix based on its superior creep resistance [15] and strength [16] at elevated temperatures. It is also interesting to note that the same $MoSi_2/Si_3N_4$ composite powder sprayed in a low pressure inert atmosphere retained very little of the $Si_3N_4$[9]. The grain size for each sample was determined from polarized light optical micrographs. Both APS and HP samples showed small $MoSi_2$ matrix grain size around the $Si_3N_4$ phase and larger grains away from the $Si_3N_4$. The APS sample had a grain size of approximately 1 to 10 μm while the HP sample had a grain size of approximately 5 to 55 μm.

To determine the steady state creep rate, the impression test was allowed to progress until the punch location was observed to vary linearly with time. The steady state punch velocity along with the punch diameter were then used to determine the creep rate according to Eq. 1. The steady state creep data collected for the APS and HP samples as a function of test temperature and applied load are shown in Fig. 2. For comparison, the creep rate of a hot-pressed monolithic $MoSi_2$ sample [14] is included in Fig. 2. The figure shows a clear dependence of creep rate on temperature and applied stress for both the APS and HP samples. In all cases the creep rate for the APS samples was higher than that for the HP samples. For the test temperature of 1200°C, the creep rate for the APS sample loaded at 370 MPa was approximately 25 times higher than for the HP sample loaded at 362 MPa. The monolithic $MoSi_2$ showed creep rates similar to the reinforced APS sample at 1200°C and similar to the reinforced HP sample at 1100°C.

The activation energies and stress exponents for the APS and HP samples were determined by curve fitting the raw data to Eq. 1. The APS sample activation energy for creep in the 1050°C to 1200°C range was 363 kJ/mol. This value was independent of

applied load. The corresponding value for the HP sample was 336 kJ/mol. Stress exponent values for the APS samples were found to depend on test temperature. For tests at 1050°C and 1100°C the stress exponent was 1.4. At 1150°C and 1200°C the stress exponent was 2.0. Stress exponents are shown in Fig. 3. Using Eq. 2 and the stress exponent values gives a value for $B$ of 2.9 and 2.4 for temperatures of 1050°C to 1100°C and 1150°C to 1200°C respectively. For the HP samples the stress exponent was found to be 4.4. Using Eq. 2 this gives a value for $B$ of 3.3. The steady state creep rates with corrected stresses (applied stress/B) are plotted in Fig. 3.

An optical micrograph of the impression area of an APS sample is shown in Fig 4. Surrounding the punch is a deviatoric stress region where the material has been expanded thus experiencing cavitation. The cavitation appears to be due to separation of the particles primarily along the original inter-splat boundaries. Movement of the punch into the sample appears to be accommodated by the movement of the individual splats with respect to each other and by some grain boundary sliding within each splat. From the figure, deformation of individual grains are not observed. The stress exponents of 1.4 and 2.0 for the APS samples suggest the dominance of a boundary type creep mechanism rather than a lattice mechanism [17]. This further supports the particle separation and movement type of boundary mechanism as observed in Fig. 4.

The impression area of the HP sample is shown in the micrograph in Fig. 5. The expansion region seen in Fig. 4 is not present in Fig. 5. Inspection of the impression region shows that the grains surrounding the punch were deformed from an equiaxed shape to an elongated shape perpendicular to the loading direction. This observation suggests creep by lattice mechanisms acting within the grains. It also appears that grain boundary sliding may be partially responsible for creep. The higher stress exponent of 4.4 for the HP sample supports the supposition of partial creep by plastic deformation of the grains [17].

Several differences between the samples are thought to be responsible for the different creep rates of APS and HP materials. One difference is the porosity of the samples. Densification of the APS sample by pore elimination under the punch was observed. This phenomena acts to accommodate creep in the APS sample but did not appear to affect the HP sample. Another difference is in the grain size of the materials. The elevated temperature creep resistance of polycrystalline $MoSi_2$ is highly sensitive to grain size.[18] The rapid solidification phenomena associated with plasma spraying results in a fine grained deposit of 1 to 10 μm. The HP sample had a much larger grain size of 5 to 55 μm. Creep dependence on grain size is most significant when grain boundary sliding is the predominant mechanism of creep. In both the APS and HP samples it appears that the grain boundary sliding mechanism is at least partially responsible for creep. Therefore, difference in grain size partially explains the lower creep rate for the HP samples.

Perhaps the largest difference between the APS and HP samples, which resulted in different creep rates, is the inter-particle bonding in the consolidated product. The weak bonding between the particles in the APS sample is evident because of the separation of

particles along splat boundaries during creep testing. Similar behavior between the consolidated particles of the HP sample was not observed due to stronger inter-particle bonding. Weak inter-particle bonding is commonly observed in APS coatings. For example, measurements of the elastic moduli of APS alumina deposits have given values five to ten times lower than those measured for the dense material [19]. Heat treatment experiments carried out on the sprayed $Al_2O_3$ samples explain the discrepancy in moduli values in terms of the imperfect bonding between splats [20]. The elastic modulus data suggest that the percent of contact area between splats which is truly bonded is approximately 25%. Direct observations carried out by electron microscopy support this result [21,22].

For comparison to the $MoSi_2/Si_3N_4$ samples tested here, compression creep rates for LPPS $MoSi_2$/SiC from ref. 6 were examined. For a test temperature of 1200°C and a load of 90 MPa the creep rate for the LPPS $MoSi_2$/SiC sample was $2.5 \times 10^{-5}$/sec. The APS $MoSi_2/Si_3N_4$ investigated here at 1200°C and a corrected load of 130 MPa gave a creep rate of $3 \times 10^{-6}$/sec. Since the compression creep rate and the impression creep rate for a corrected load show good agreement [14], the APS $MoSi_2/Si_3N_4$ in this investigation was somewhat more creep resistance than the LPPS $MoSi_2$/SiC material reported in Ref. 6. Since it is expected that inter-particle bonding is stronger in the LPPS sample, the improved creep resistance of the APS material may be attributed to a higher reinforcing phase content (combining the reinforcing effect of both the $Mo_5Si_3$ and the $Si_3N_4$), a finer and/or more uniform distribution of the reinforcing phase, a grain size effect, or a decrease in the glassy silica phase content at grain boundaries. Since the silica phase was not directly observed in this study or the study described in Ref. 6, its relative effect on the creep behavior of the APS and LPPS samples is uncertain.

## Conclusions

Samples of high temperature reaction synthesized $MoSi_2/Si_3N_4$ powder consolidated by atmospheric plasma spraying (APS) and hot pressing (HP) were impression creep tested in the temperature range of 1000°C to 1200°C. The APS samples showed creep by sprayed particle sliding and grain boundary sliding. The stress exponents of 1.4 and 2.0 of the APS material further suggested a boundary type creep mechanism. The HP samples showed creep by grain deformation with possible grain boundary sliding. The stress exponent of 4.4 for the HP samples suggested that a lattice type creep mechanism was more prevalent than in the APS samples. The HP material demonstrated superior creep resistance as compared to the APS material due primarily to stronger inter-particle bonding and larger grain size. However, the APS $MoSi_2/Si_3N_4$ material tested in this investigation showed improved creep resistance compared to LPPS $MoSi_2$/SiC results reported previously. Further investigation of the retention of $Si_3N_4$ in APS versus LPPS deposits is planned to explain the higher retained reinforcing phase in the APS sample.

## References

1. J.J. Petrovic, MRS Bulletin, 18, (7),p. 35-40, July 1993.
2. J. Schlichting, High Temp. High Pressures, 10, 241 (1978).
3. E. Fitzer, R. E. Tressler and M. McNallan (eds.), "Corrosion and Corrosive Degradation of Ceramics," p 19, American Ceramics Society, Westerville, OH (1989).
4. T. A. Kircher, E. L. Courtright, Mater. Sci. Eng., A155, 67-74 (1992).
5. Y.L. Jeng, J. Wolfenstine, E.J. Lavernia, D.E. Baily, A. Sickinger, Scripta Metallurgica Et Materialia, 28, 453-458 (1993).
6. Y.L. Jeng, E.J. Lavernia, J. Wolfenstine, D.E. Baily, A. Sickinger, Scripta Metallurgica Et Materialia, 29, 107-111 (1993).
7. E. Heikinheimo, A. Kodentsov, J.A. Van Beek, J.T. Klomp, and F.J.J. Van Loo, Acta Metall. Mater., 40, S111-S119 (1992).
8. M.G. Hebsur, Mat. Res. Soc. Symp. Proc., 350, 177-182 (1994).
9. A.H. Bartlett, R.G. Castro, submitted to Journal of Materials Science.
10. Z.A. Munir, V. Anselmi-Tamburinia, Mater. Sci. Reports, 3, 277 (1989).
11. H. Kung, Y-C Lu, A.H. Bartlett, R.G. Castro, J.J. Petrovic, to be published in J. Materials Research.
12. S.N.G. Chu and J.C.M. Li, J. Mater. Sci., 12, 2214 (1977).
13. S.N.G. Chu and J.C.M. Li, Mater. Sci. Eng., 39, 1 (1979).
14. D.P. Butt, D.A. Korzekwa, S.A. Maloy, H. Hung, J.J. Petrovic, J. Mater. Res., 11, 1528-1536 (1996).
15. D.P. Mason, D.C. Van Aken, Acta Metall. Mater., 43, 1201-1210 (1995).
16. R.G. Castro, H. Kung, P.W. Stanek, Mater. Sci. Eng., A185,65-70 (1994).
17. A.G. Evans and T.G. Langdon, Progress in Materials Science, 21, 370 (1976).
18. R. Doralia (ed.), p. 809, "Structural Intermetallics," p. 809, TMS/AIME, Warrendale, PA. (1993).
19. D. Fargeot, F. Platon and P. Boch, Sci. Ceram., 9, 48 (1977).
20. R. McPherson, B.V. Shafer, Thin Solid Films, 97, 201-204 (1982).
21. A. Ohmori, C.J. Li, Y. Arata, in Proc. Fourth. Nat. Thermal Spray Conf., Pittsburgh, May 1991, p.105-113.
22. S. Boire-Lavigne, C. Moreau, and R.G. Saint-Jacques, 32nd Ann. Conf. of Metallurgists, CIM, (1993), pp. 473-485.

**Acknowledgment**

This research was funded through the DOE office of Advanced Industrial Materials. Los Alamos National Laboratory is operated by the University of California.

Table 1. APS Spray Parameters for $MoSi_2/Si_3N_4$ composite material.

| | |
|---|---|
| Plasma Torch | Miller SG1B |
| Voltage | 24V |
| Current | 625A |
| Arc Gas Flow (Ar) | 28 SLM |
| Powder Gas Flow (Ar) | 5 SLM |
| Spray Distance | 100 mm |

Table 2. Hot-Pressing Parameters for $MoSi_2/Si_3N_4$ composite material.

| | |
|---|---|
| Powder Weight | 30 g |
| Die Diameter | 32 mm |
| Pre-Press Temperature/Time | 1200°C / 5 min. |
| Pre-Press Pressure | 1.95 MPa |
| Hot-Press Temperature/Time | 1800°C / 5 min. |
| Hot-Press Pressure | 1.95 MPa |
| Atmosphere | Ar |

Table 3. Sample composition from image analysis.

| | *APS sample* | *HP sample* |
|---|---|---|
| porosity (volume %) | 10% | 2% |
| $Si_3N_4$ (volume %) | 20% | 19% |
| $Mo_5Si_3$ (volume %) | 7% | 2% |

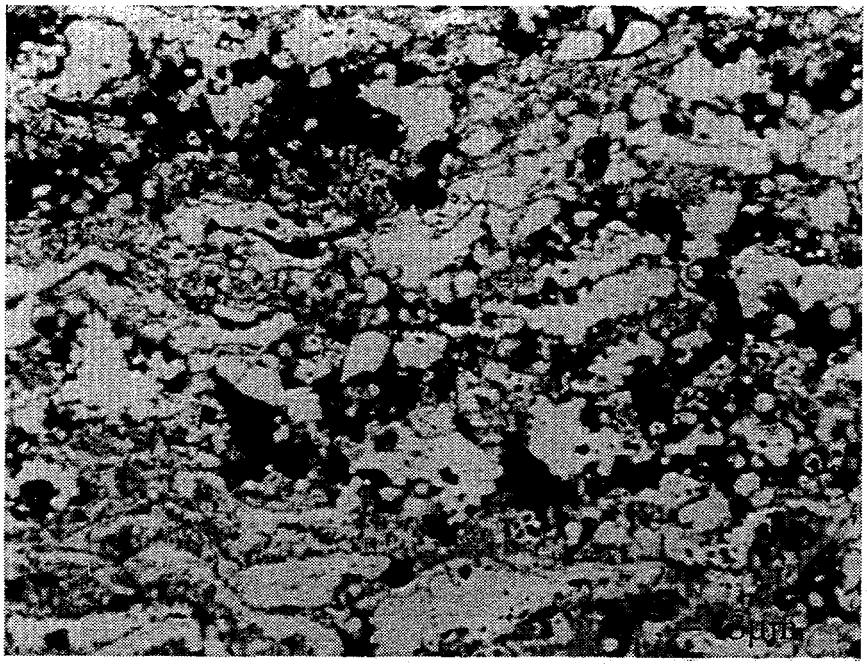

Figure 1. Optical micrograph of an APS $MoSi_2/Si_3N_4$ sample showing the distribution of $MoSi_2/Mo_5Si_3$ (lightest phase), $Si_3N_4$ (gray phase), and porosity (darkest phase).

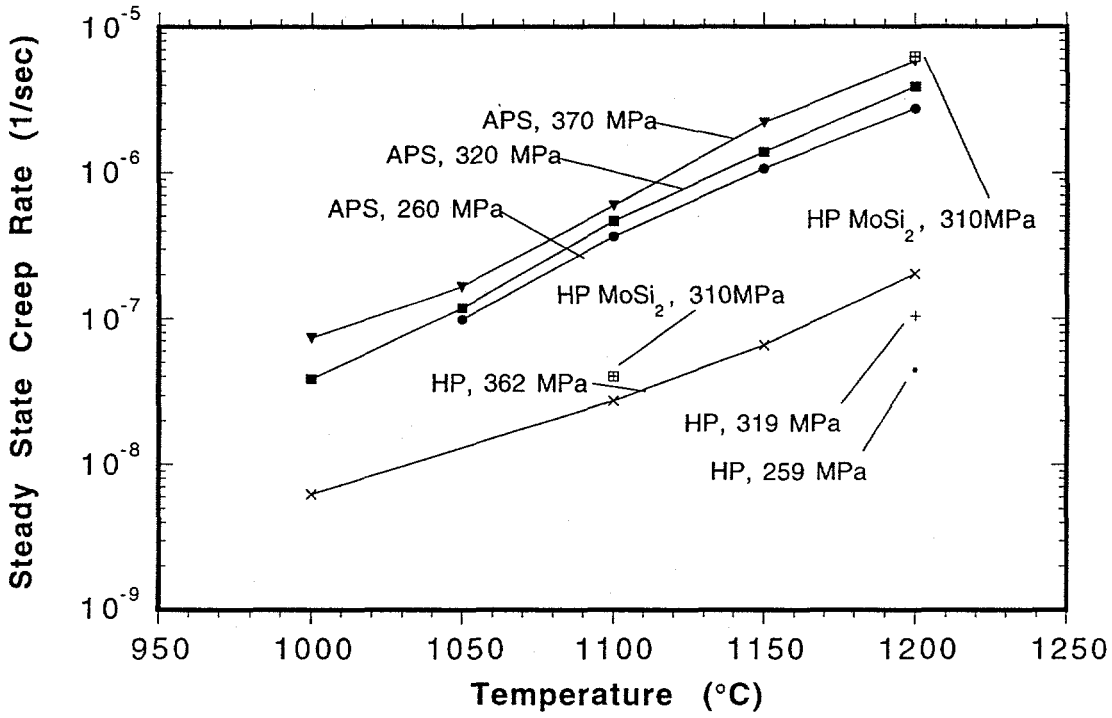


Figure 2. Steady state creep rate as a function of temperature and applied stress for APS and HP $MoSi_2/Si_3N_4$ composite samples. Monolithic $MoSi_2$ data points from Ref. 14 shown for comparison.

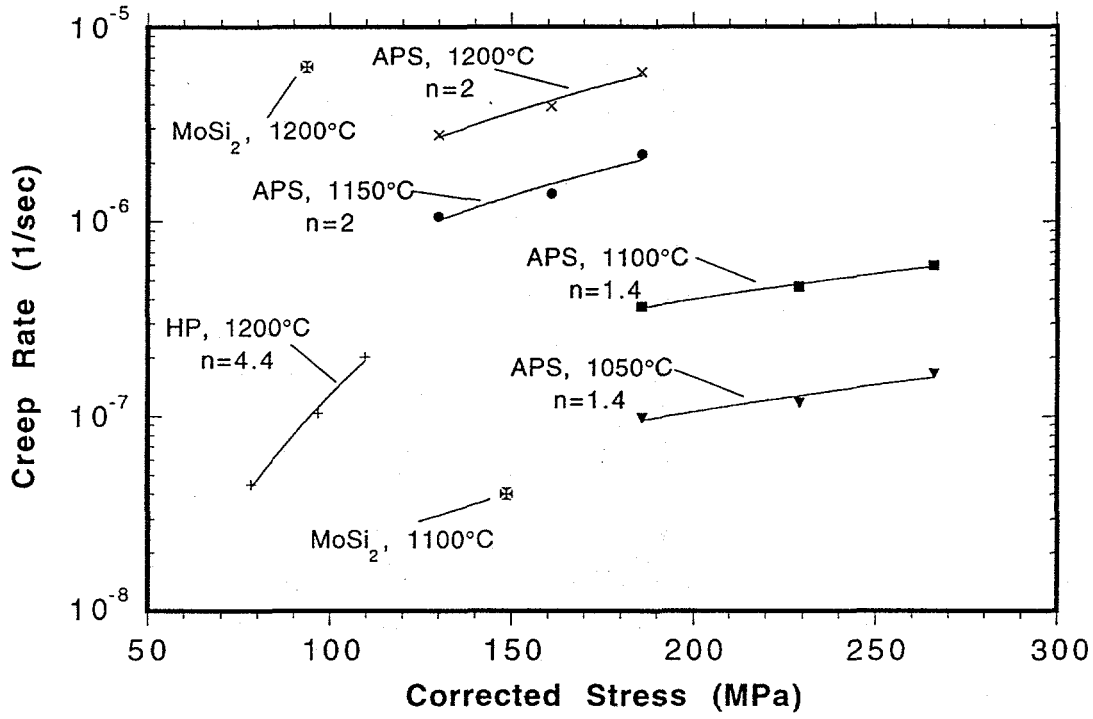


Figure 3. Steady state creep rate as a function of corrected load and temperature for APS and HP $MoSi_2/Si_3N_4$ composite samples. The power curve fits show stress exponent calculation. Monolithic $MoSi_2$ data points from Ref. 14 shown for comparison.

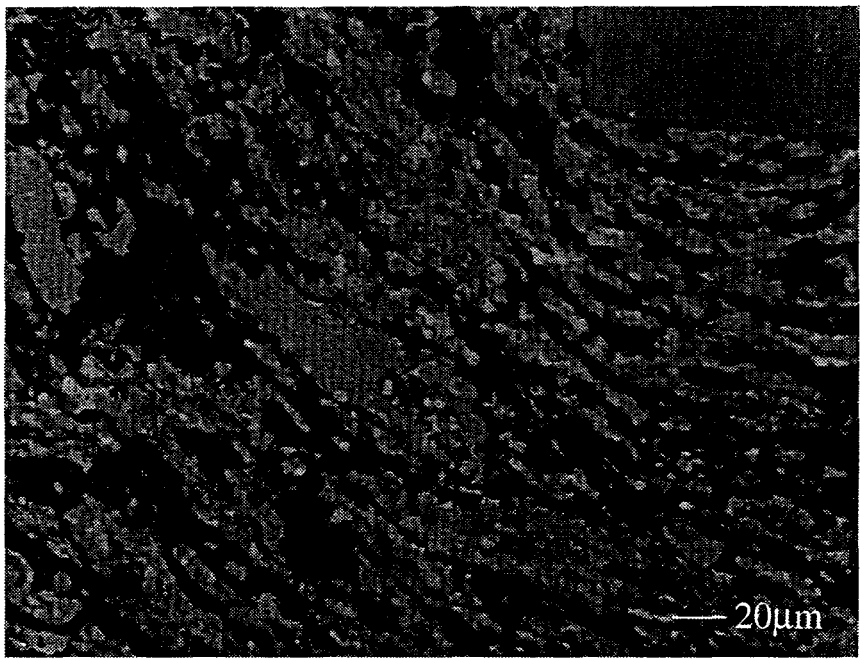


Figure 4. Punch region of APS sample after creep test has concluded. Note punch in upper right corner.

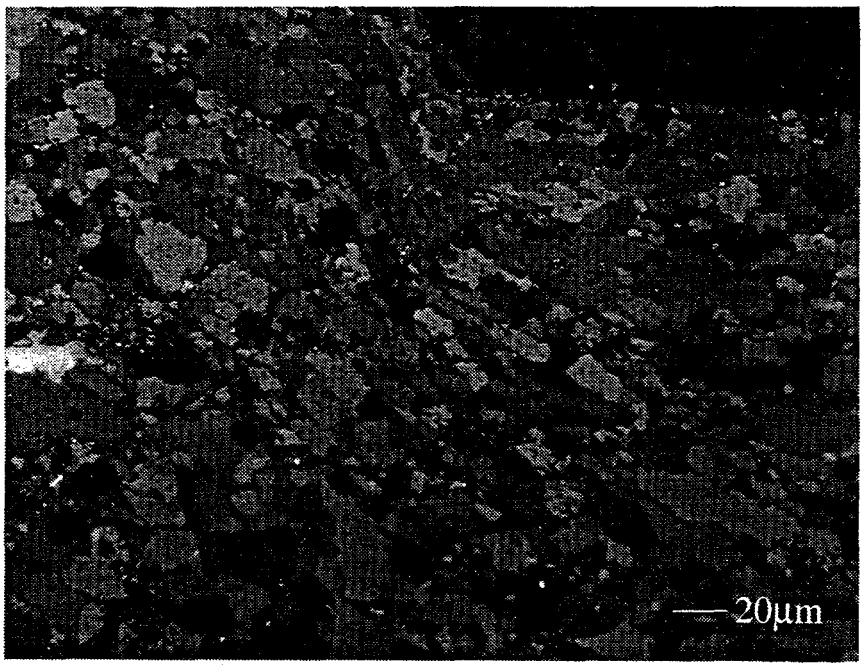


Figure 5. Punch region of HP sample after creep test has concluded. Note punch in upper right corner.